

Study within the Mining Effects Knowledge Program (KEM-39) on the cyclic storage of gases in the Netherlands

WP1: A review on the influence of CO₂, H₂ and N₂ storage in the evolution of fault properties and induced seismicity

Authors:

Eng. Isotton Giovanni¹
Prof. Janna Carlo¹
Prof. Teatini Pietro¹
Prof. Deangeli Chiara²
Prof. Rocca Vera²
Prof. Verga Francesca²
Prof. Collettini Cristiano³

Affiliations:

¹M3E srl
²Politecnico di Torino
³Università la Sapienza

Document type: Technical report

Date: December 2022

INDEX

1	Intro.....	3
2	Simple Mechanics of Induced Earthquakes	3
3	Mechano-chemical effects of CO ₂ on fault rocks	4
4	Important lessons for induced seismicity from different case studies	7
5	Summary of lessons from the case studies of induced seismicity reported in this document ..	23
	References.....	24

I Intro

In the last 10-15 years, large areas considered geologically stable with little or not detected seismicity have become seismically active. The most impressive example is represented by Oklahoma where the rate of occurrence of earthquakes with magnitude, $M > 3.0$, exceeded that of California (McGarr et al., 2015). To a large extent, the increasing rate of earthquakes is due to activities used in modern energy production (Ellsworth 2013; McGarr et al., 2015). These activities include: a) wastewater disposals into deep geological formations; b) injection of water or CO_2 into depleted reservoir for enhanced oil recovery (EOR); c) hydraulic fracturing to enable production of oil and gas from low permeability reservoir; d) injection of CO_2 into deep formations for permanent carbon capture and storage (CCS); e) injection into geothermal reservoir to develop enhanced geothermal systems (EGS); f) gas pressure depletion and associated compaction of the rocks forming the reservoir.

In the seminal paper of Ellsworth (2013) it is reported that induced earthquakes sometimes occur at the source of the stress or pressure perturbation and at other times, these events take place deep below and kilometers away from the source. Sometimes induced events occur shortly after the industrial activity begins, but in other cases they happen long after it has been under way or even ceased. Factors that should enhance the probability of a particular stress or pore-pressure perturbation inducing earthquakes include the magnitude of the perturbation, its spatial extent, ambient stress condition close to the failure condition, and the presence of faults well oriented for failure in the tectonic stress field. Hydraulic connection between the injection zone and faults in the basement may also favor inducing earthquakes, as the tectonic shear stress increases with depth in the brittle crust. In addition, the larger the fault, the larger the magnitude of earthquakes it can host. However only a small fraction of the wells used for geo-energy production appear to be problematic (Ellsworth 2013; McGarr et al., 2015).

2 Simple Mechanics of Induced Earthquakes

A fault will remain locked as long as the applied shear stress is less than the fault strength. The basic physical mechanism for inducing seismicity is well understood in terms of the effective stress principle:

$$\tau = C + \mu(\sigma_n - P_f) \quad (1)$$

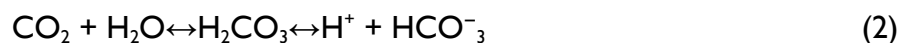
where τ is the shear stress acting on the fault, C is cohesion, and μ is the coefficient of friction which is multiplied by the difference between the normal stress (σ_n) and fluid pressure (P_f), which represents the effective normal stress (σ_n').

The terms of Equation (1) can change mainly as a function of two main processes operating at different timescales. In the short term, i.e. during the injection period that can last up to decades, increasing the shear stress, reducing the normal stress, and/or elevating the pore pressure can bring the fault to failure, triggering the nucleation of earthquakes. In the long-term, for example during the CO_2 storage phase with time scale of several thousand years, fluid-rock interactions can change the fault rock fabric and mineralogy, with possible associated changes in frictional properties, and/or favor dissolution and cementation processes with the associated increase of fault cohesion.

In the following we will present some mechano-chemical effects of CO_2 on fault rocks with some indications also for H_2 and N_2 . Then we will analyze some case studies that provided important lessons for induced seismicity.

3 Mechano-chemical effects of CO_2 on fault rocks

Although pure dry CO_2 has low reactivity, once it comes into contact with brine, it forms H_2CO_3 , a weak acid that will almost immediately dissociate in (Gaus et al., 2008):



producing a reduction of the pH of the formation from near neutral to acid values in the range 4–5. This reaction can potentially cause acid reactions within the minerals of the fault rock. A comparison of laboratory friction test where: a) the fault rock was in contact with CO_2 for several hours and b) for samples exposed to CO_2 on natural time scales of millions of years, i.e. samples taken from natural analogues, show a limited tendency for a reduction in friction due to the CO_2 exposure (Fig. 1 and Rohmer et al., 2016).

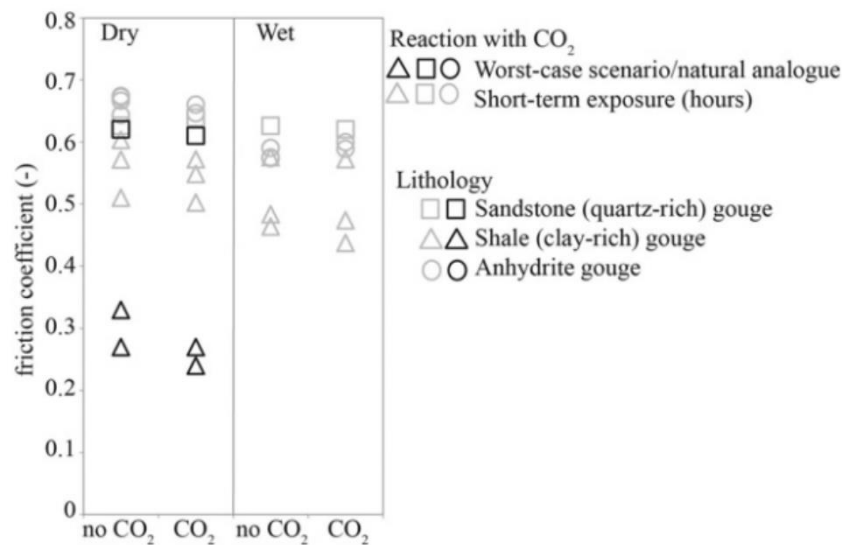


Figure 1. Friction coefficient for a fault gouge with or without CO₂ (Rohmer et al., 2016).

To the best of our knowledge there are not laboratory studies showing how CO₂-enhanced dissolution and re-precipitation processes influence fault cohesion. However, field studies on exhumed faults showing at the surface fault processes occurring at depth, demonstrate that in area characterized by a large CO₂ degassing fault cohesion can be regained by fluid-assisted cementation processes (Collettini et al., 2008).

The analysis presented via equation 1 document the role of fluid pressure in fault reactivation, but it does not address the question of slip behaviour, seismic or aseismic, upon fault reactivation. Elastic dislocation theory combined with rate-and-state friction constitutive equations provide a more comprehensive analysis of fault stability (Scholz, 2019). In particular in the lab some velocity steps are performed to characterize the velocity dependence of friction, quantified by the (a-b) parameter. Positive values of (a - b) indicate velocity-strengthening behavior, that favors stable sliding and fault creep. Negative values of (a - b) represent a velocity-weakening behavior, that is a requirement for the nucleation of slip instability. In short-term laboratory experiments, where it is considered only the effect of increasing pore-fluid pressure due to CO₂ injection and not possible mineral alterations due to long-term fluid rock interaction, it has been shown that fault stability is not affected by CO₂ storage (Samuelson and Spiers, 2012). In particular, 3 caprock samples, 1 reservoir rock, and 1 mixture of reservoir and caprock belonging to a potential pilot for CO₂ sequestration within a reservoir situated in the Netherlands sector of the North Sea, have been tested. The friction rate

parameter ($a-b$) measured in low shear velocity steps (0.2–1–10–1–0.2 $\mu\text{m/s}$) indicates that all tested materials exhibit predominantly velocity strengthening behavior, and that neither the addition of brine nor supercritical CO_2 has any clear, strong influence on friction velocity dependence (Fig. 2). Only the sample in figure 2D and 2E show any tendency towards velocity weakening ($a - b < 0$), evident only in those experiments with CO_2 . In each case the only measurement in which ($a - b$) < 0 is on the final velocity step, suggesting that this tendency towards velocity weakening may be more a function of strain than of the presence of CO_2 (Samuelson and Spiers, 2012).

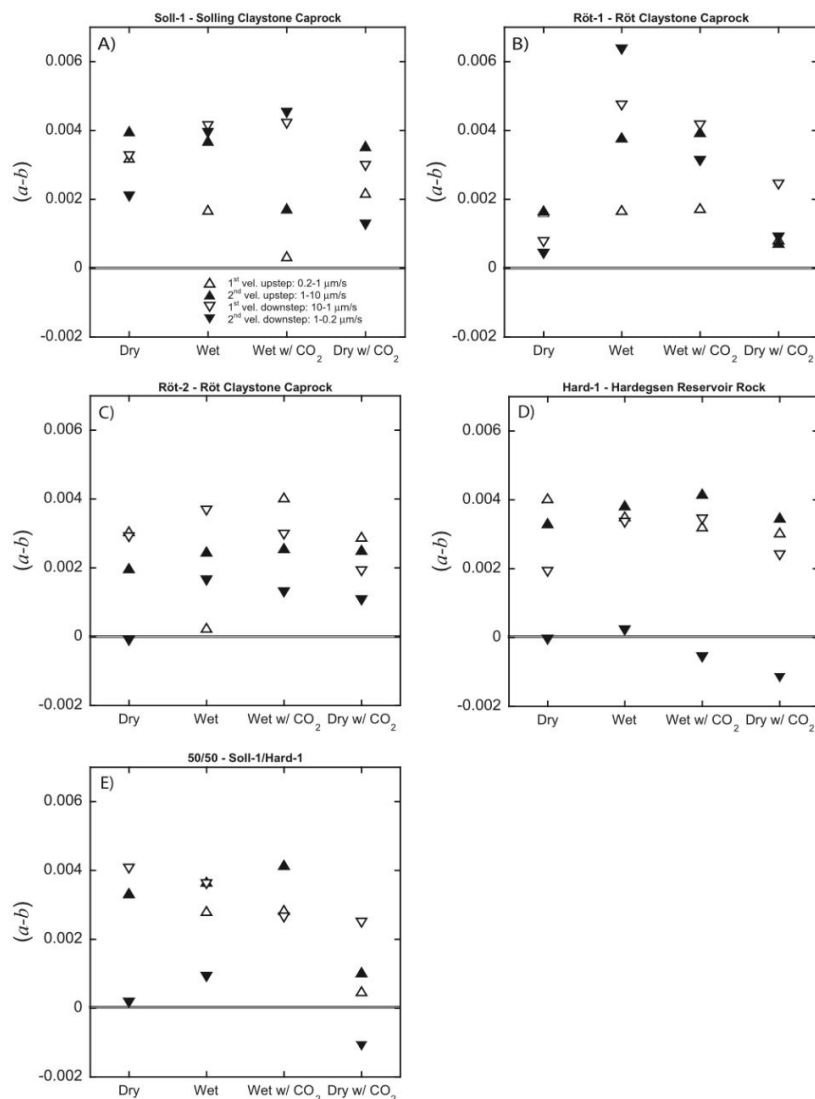


Figure 2. Limited effect of CO_2 in the friction rate parameter ($a-b$), from Samuelson and Spiers (2012).

Experience with underground hydrogen storage in porous geological formations is very limited (Heinemann et al., 2021) and practical applications are restricted to the storage of town gas, i.e. gas mixtures with 25–60% hydrogen, and smaller amounts of CH₄ (10–33%), CO and CO₂ (12–20%) and <30% N₂. Town gas storage has been utilised in aquifers in France (Beynes), Czechoslovakia (Lobodice) and Germany (Engelborstel, Bad Lauch- staedt, Kiel). Therefore, the influence of H₂ and N₂ in in the evolution of fault frictional properties and fault cohesion is not documented. Hydrogen injected into a porous reservoir will change the chemical equilibrium between the formation pore water promoting fluid-assisted, grain–scale processes. Such processes include local grain–contact cement dissolution, clay mineral sorption/desorption within grain boundaries, fluid-assisted slow crack growth (stress corrosion cracking), dissolution–precipitation and/or inter- granular frictional slip (Heinemann et al., 2021). Although the above-mentioned grain–scale mechanisms are well studied, little is known about the influence of hydrogen and nitrogen on their rates.

4 Important lessons for induced seismicity from different case studies

Unless there are medium and/long term chemical reactions that can affect the fault frictional and fluid-flow properties, the usual mechanisms of pore pressure elevation, aseismic fault activation and stress transfer are the ones to worry about for induced seismicity. In the following we will report on some case-studies that provided important lessons. We will focus on:

- a) Induced seismicity of the Groningen gas field
- b) Wastewater fluid disposals inducing earthquakes on basement faults (Oklahoma seismicity)
- c) Different EGS stories: Helsinki (Finland, $M_{\max} = 1.7$) vs. Pohang (Korea, $M_{\max} = 5.5$)
- d) b -values analyses to discriminate between on-fault vs distributed seismicity during fracking
- e) The role of aseismic slip and earthquake triggering
- f) $M_w = 4.1$ during CO₂ sequestration at Castor site, Spain, revisited
- g) CO₂ storage sites with limited induced seismicity

a) Induced seismicity of the Groningen gas field

One of the world's best-known gas fields showing production-induced compaction, subsidence, and seismicity is the vast Groningen field, the Netherlands. The reservoir is the 100–350-m-thick Slochteren Sandstone, located at about 3 km depth, where the overburden pressure is ~65 MPa (Van Eijs, 2015). Since gas production started in the 1960s, gas pressure has fallen from 35 to ~8 MPa, and subsidence, driven by the increase in vertical effective stress, has reached ~33 cm in the center of the field (Verberne et al., 2020). Subsidence is caused by one-dimensional (1-D) vertical compaction of the reservoir rock, whereas seismicity reflects coupled stress buildup on preexisting faults (Segall, 1989). The first earthquake felt in the Groningen area occurred in 1991 ($M_L = 2.4$) and in the subsequent 10 years, induced seismicity stayed at a rate of about five events ($M_L \geq 1.5$) per year (Thienen-Visser and Breunese, 2015). From 2003, the number of events and magnitudes started to increase. Observed magnitudes of the induced earthquakes in Groningen are usually in the range $0.5 < M_L < 3.0$ except for a few stronger events: one with magnitude 3.5 that occurred on 2006 August 8, while the largest event recorded was the magnitude 3.6 on 2012 August 16 (Spetzler and Dost, 2017).

The densification of the seismic network together with an accurate local seismic velocity model allowed an improvement of epicentral accuracy from 0.5–1 km to 0.1–0.3 km and a vertical resolution of about 0.3 km (Dost et al., 2017). A limited number, 87, of relocated earthquakes recorded from 2014 to 2016 have shown that seismic activity is mostly concentrated within the known faults, trending NW-SE and E-W, and it occurs within the reservoir formations (Fig. 3 and Spetzler and Dost, 2017).

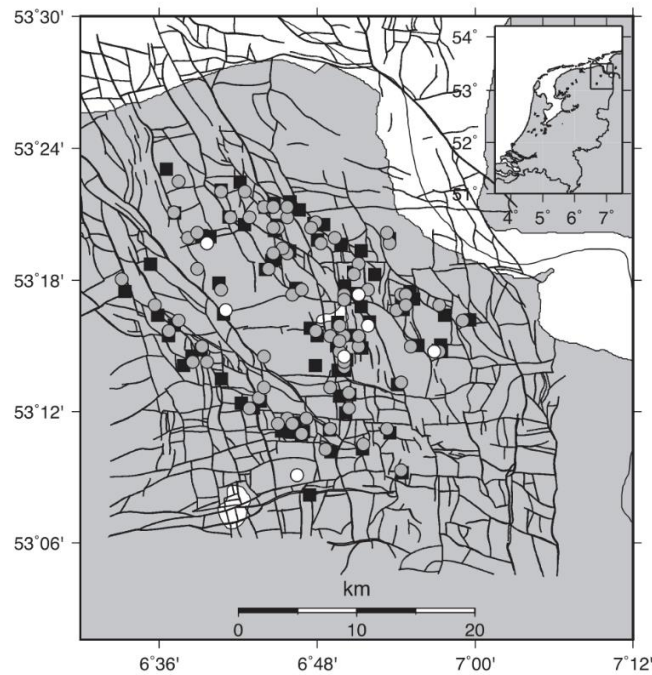


Figure 3. Earthquake distribution within the Groningen gas field: black square are earthquakes located with the hypocenter method whereas earthquakes located with differential travel time method are reported as gray and white circles. NW–SE and E–W aligned fault systems are illustrated with black lines (from Spetzler and Dost, 2017).

Earthquake focal mechanisms obtained from events recorded by a shallow borehole network between 2015 and 2017 show a predominant extensional kinematics with NW-SE trending nodal planes that are consistent with the major faults detected in the area (Fig. 4 and Willacy et al., 2018).

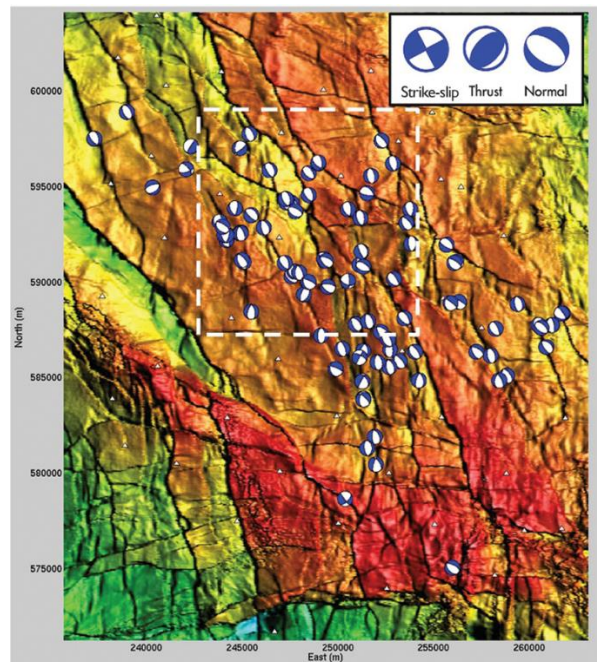


Figure 4. Focal mechanisms for earthquakes recorded by a shallow borehole array between 2015 and September 2017 (from Willacy et al., 2018).

b) Wastewater fluid disposals inducing earthquakes on basement faults (Oklahoma seismicity)

Since about 2009, a large number of earthquakes struck Oklahoma and adjacent states. It is now generally accepted that this seismicity is caused by large-scale wastewater injection (Ellsworth et al., 2015; Walsh and Zoback, 2015). Wastewater is disposed into more than 800 wells drilled into the high-permeability Arbuckle Group. Addition of fluid creates a far-reaching plume of modestly elevated pore pressure (<2 MPa) relative to the natural underpressured state of the Arbuckle. Permeable pathways from the Arbuckle into the basement raise the pressure in hydrologically connected basement faults, reducing their strength through the reduction of the effective stress (Fig. 5). Earthquake sequences have been observed several tens of kilometers away from large injectors in Oklahoma where modeled effective stress changes at hypocentral depth are less than 0.5 MPa (Keranen et al., 2014). Because of the many active disposal wells and the far-reaching pressure perturbation, it is generally impossible to associate induced sequences with injection activity of specific wells. The occurrence of induced seismicity within the basement rocks of Oklahoma, promoted by very small fluid pressure perturbations, $\Delta p < 0.5$ MPa, reinforces the concept of

critically stressed faults within the crust (Zoback and Townend, 2000) where small fluid pressure and/or stress perturbation can generate earthquakes.

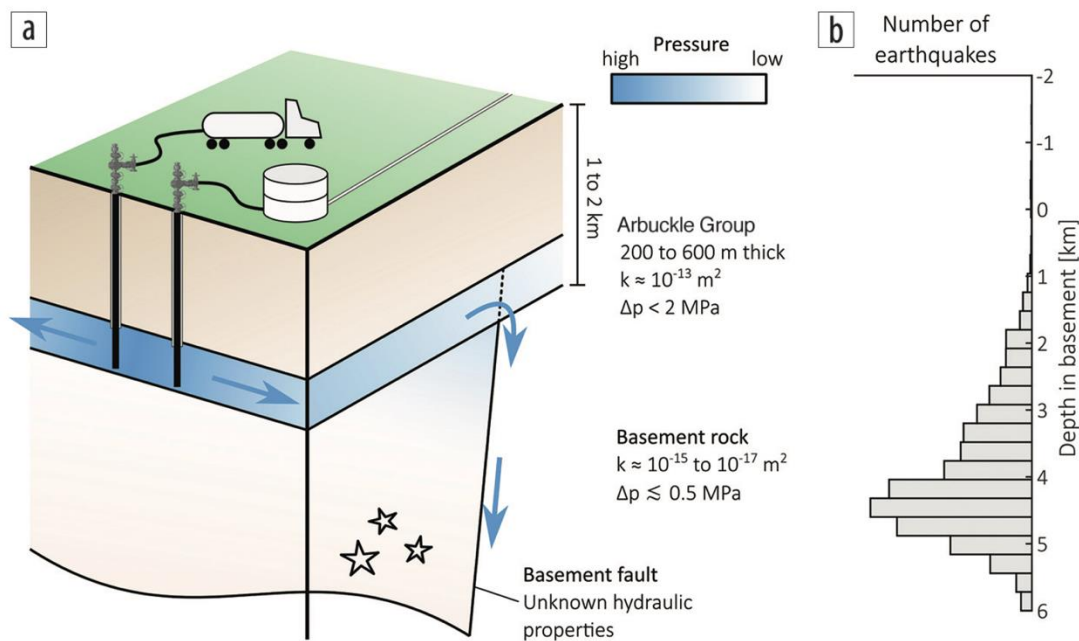


Figure 5. Conceptual model of induced seismicity in Oklahoma and southern Kansas, from Schoenball et al., 2018.

c) Different EGS stories: Helsinki (Finland, induced seismicity likely to be limited by changes in pumping strategy) vs. Pohang (Korea, a triggered $M = 5.5$ promoted by a run-away rupture)

HELSINKI (FINLAND)

During the stimulation of a 6.1-km-deep geothermal well near Helsinki, Finland, near-real-time seismic monitoring of fluid injection allowed control of induced earthquakes (details in Kwiatek et al., 2019). Seismic monitoring was performed by a local network integrated with a 24-station borehole seismometer network (OTN-2 in Fig. 6) allowing high-precision, near-real-time monitoring and analysis of seismic data feeding a traffic light system (TLS). In the case study of Helsinki, the adjustment of the stimulation schedule to the observed evolution of induced seismicity allowed to successfully prevent the occurrence of larger $M > 2.0$ events (Kwiatek et al., 2019).

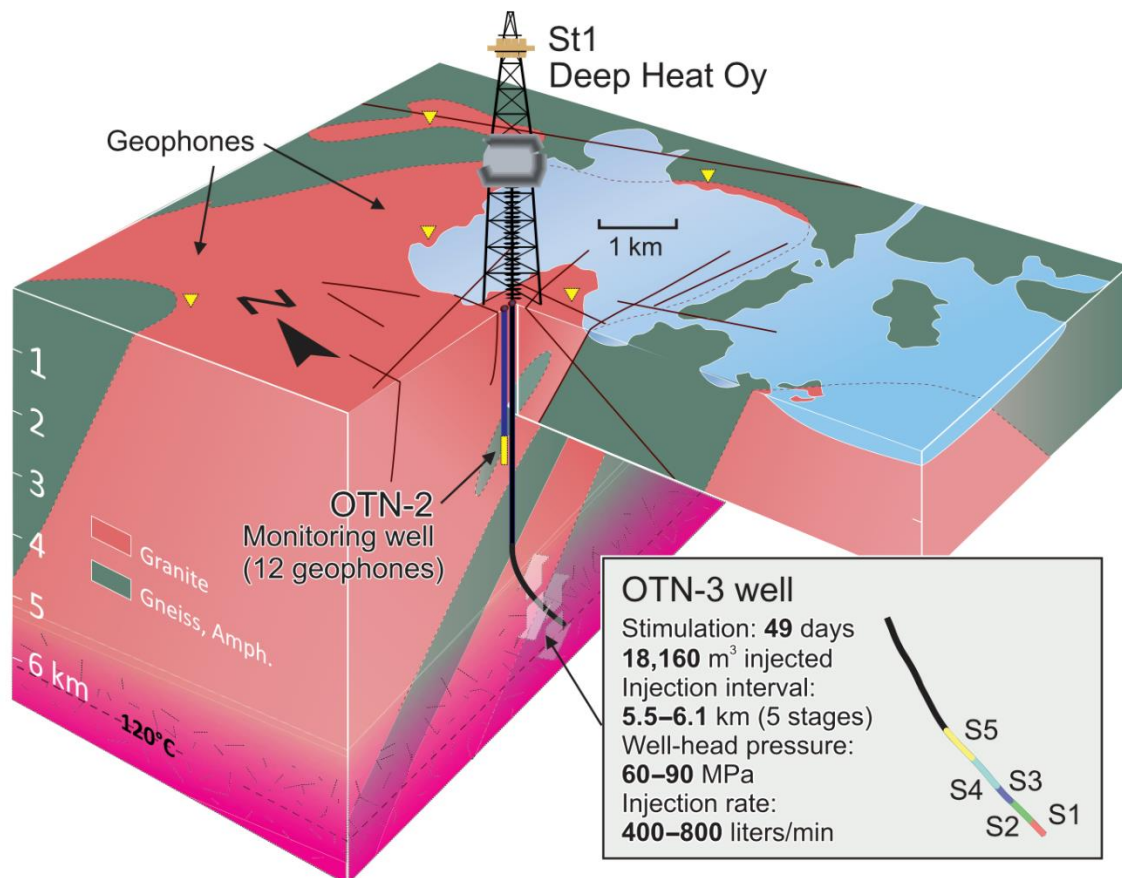


Figure 6. Schematic representation of the Helsinki EGS project (from Kwiatek et al., 2019).

Induced seismicity showed a monotonic increase of maximum earthquake magnitude with the cumulative injected fluid volume (Fig. 7). This increase followed the trend predicted by the recently introduced fracture mechanics–based model of Galis et al. 2017. According to Galis et al., this behavior suggests that the maximum magnitude depends on both the regional tectonic stress and the imposed local fluid pressure controlling the total elastic energy stored in the system. Considering the observed trend in maximum magnitude evolution with the injected fluid volume, the pumping strategy was modified following phase P2 (Fig. 7). In particular: a) well-head pressures were limited to about 86 MPa; b) injection subphases of P4 and P5 were reduced in duration to 18 hours with 6-hour rest periods; c) pumping was immediately stopped and resting periods extended whenever a large seismic event with $M_w > 1.7$ occurred. According to the authors (Kwiatek et al., 2019) the adopted procedure avoided the nucleation of a project-stopping magnitude $M_w = 2.0$ induced earthquake, a limit set by local authorities. However, it is possible that the advantageous geological

and tectonic reservoir features and favorable stress conditions of the test-site contributed to project success. Therefore, similar procedures have to be adopted in other tectonic settings to better asses to control on fluid-induced seismicity.

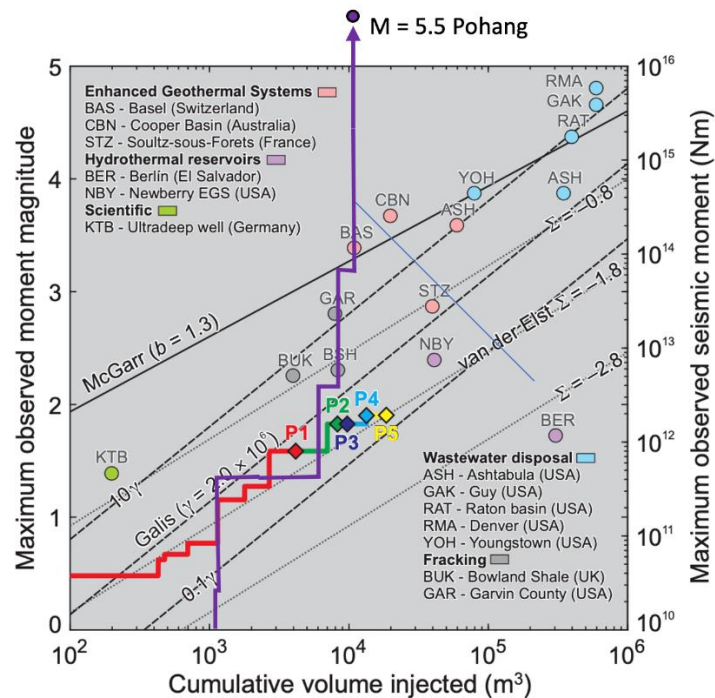


Fig. 7 Different paths of cumulative injected volume vs. maximum observed moment magnitude for Helsinki (red/green/blue path) and Pohang (purple path). Modified from Kwiatek et al., 2019.

POHANG (KOREA)

On November 2017, the city of Pohang, Korea, was affected by a magnitude 5.5 earthquake occurred in the vicinity of the first Republic of Korea's first enhanced geothermal system (EGS). The Pohang EGS project was intended to create an artificial geothermal reservoir within low-permeability crystalline basement by hydraulically stimulating the rock to form a connected network of fractures between two wells, PX-1 and PX-2, at a depth of ~4 km (Fig. 8).

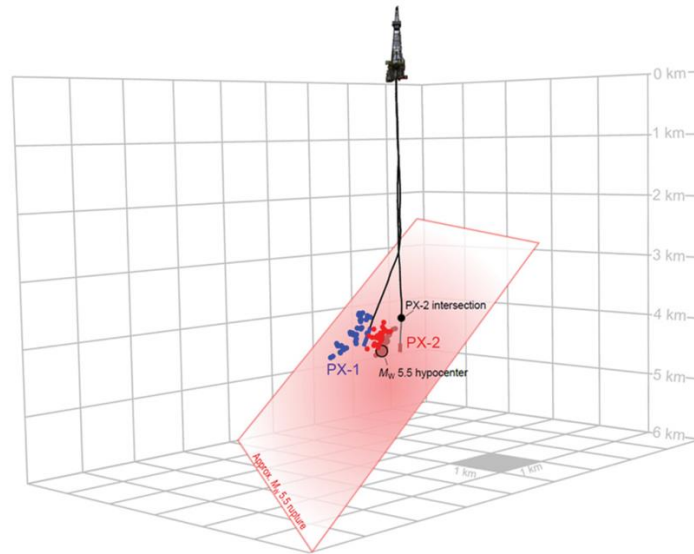


Figure 8. Schematic illustration of the sequence of seismicity associated with stimulation of PX-1 and PX-2. The red area represents the rupture area of the $M_w = 5.5$ Pohang earthquake (Ellsworth et al., 2019).

The analysis of an Overseas Research Advisory Committee (ORAC), asked to define whether the EGS stimulations had triggered the $M = 5.5$ earthquake was the following: “*The Pohang earthquake was triggered by the EGS stimulation of the PX-2 well. Seismicity induced by injection activated a previously unknown fault, which in turn triggered the mainshock*” (Ellsworth et al., 2019).

The comparison of the two examples of EGS triggered seismicity, indicates that differences in tectonics, reservoir and stress conditions can produce significantly different earthquake magnitudes. The behaviour observed for Helsinki is an indication for stable growth of self-arrested ruptures. In this scenario the size of the earthquakes is likely governed by the induced pore pressure perturbation. If the pore pressure, that is, the injected volume or applied hydraulic energy, grows, so does the rupture area. This would result in constantly increasing magnitudes and cumulative moment with injected volume (red/green/blue path in Fig. 7). The Pohang seismic sequence shows a steep increase of maximum magnitude. This trend is not captured by any of the models (McGarr, van der Elst, Galis, purple path in figure 7) and suggest activation of runaway ruptures (Bentz et al., 2021). A runaway rupture is a rupture initiated by anthropogenic forcing that grows in size beyond

the bounds of the stimulated region and it releases tectonic strain. The rupture size is only limited by the size of tectonic faults.

The comparison of the two dataset indicates that near–real-time monitoring, and analysis of seismic data are crucial to find a possible road to controlling stimulation-induced seismicity.

d) *b*-values to discriminate between on-fault vs distributed seismicity during hydraulic fracturing in Horn River Basin (HRB), British Columbia, Canada.

The frequency-magnitude distribution of earthquakes is usually modelled with an exponential function, called Gutenberg-Richter law, written as: $\ln N(M) = a - bM$, where $N(M)$ represents the number of events with magnitude larger than M , a is the productivity and b controls the relative rate of small and large earthquakes. In general, *b*-value shows an inverse dependence on differential stress (Schorlemmer and Wiemer, 2005), it increases on increasingly rough faults (Goebel et al., 2017), and during earthquake swarms high *b*-values are linked to fluid diffusion and reactivation of numerous small faults (Shelly et al., 2016). For some seismic sequences a near real-time characterization of the *b*-value (Gulia and Wiemer, 2019) has been used to discriminate between foreshocks (decreasing *b*-values) and aftershocks (increasing *b*-values). However, the influence of structural complexities and expert judgment on the outcome of the analysis limit the use of *b*-value evolution for earthquake forecasting (Cousineau et al., 2020).

Microseismic data acquired during a multi-well, multistage hydraulic fracture treatment conducted in the HRB have been recorded and analyzed by Kettlety et al., 2019. The dataset consists of 92.700 microearthquakes with magnitudes ranging from $-2.4 < MW < 0.5$. The events have been clustered on the grounds of their spatial position and for each cluster the *b*-value has been calculated. The distribution of *b*-values is bimodal (Fig. 9). Most event clusters have high *b*-values ($b > 1.5$), implying that they are associated with normal hydraulic fracture propagation, while a smaller number of clusters have $b \approx 1.0$, a value like tectonic earthquake sequences, suggesting that they are the result of the reactivation of pre-existing faults (Kettlety et al., 2019).

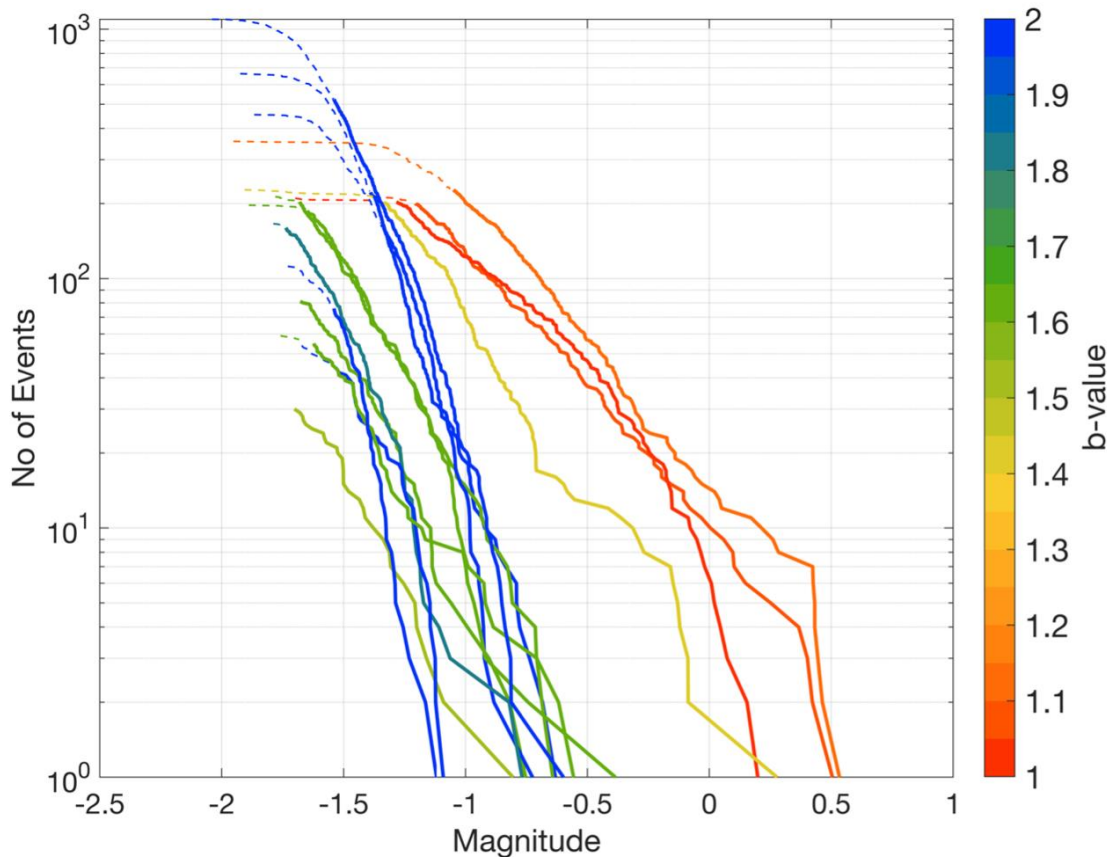


Figure 9. Frequency-magnitude distribution of microearthquakes recorded during hydraulic fracturing within the Horn River Basin (Kettlety et al., 2019).

e) The role of aseismic slip and earthquake triggering.

Models for hydraulic fracturing–induced earthquakes in shales typically ascribe fault activation to elevated pore pressure or increased shear stress. However, these mechanisms for earthquake nucleation are incompatible with experiments and physical models based on rate and state friction, which predict stable sliding and fault creep within the velocity strengthening clay-rich lithologies (Scuderi and Collettini 2018). A new gamut of models explains the induced seismicity not directly generated by the increasing fluid pressure, but rather triggered by the stress perturbations transferred from the aseismic motion within velocity strengthening fault rocks, caused by the injection. In the following we are presenting some examples of fault reactivation promoted by fluid injection where aseismic slip exerts a primary role in inducing seismicity.

During hydraulic fracturing within the clay-rich Duvernay formation in central Alberta, Canada, the increase of pore pressure promoted aseismic creep. The time-space evolution of the seismicity shows an updip progression leading up to the Mw 4.1 earthquake. Eyre et al., 2019 proposed that from the Duvernay formation an upward propagation of fault creep promoted a dynamic rupture where the deformation front impinges on regions of the fault hosted within velocity weakening material (Fig. 10).

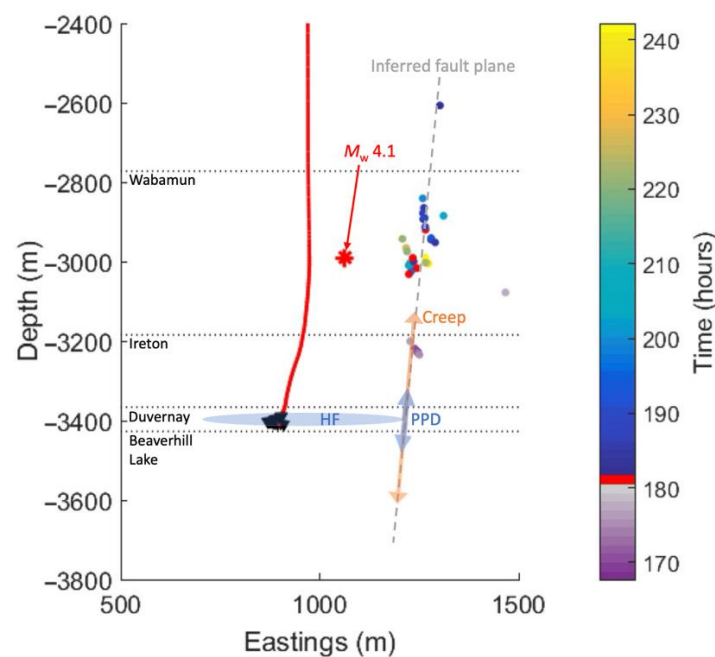


Figure 10. Foreshocks and aftershocks of the Mw 4.1 earthquake over time in cross section. The mainshock is believed to be located on the same fault plane as the other events but is slightly mislocated horizontally because of the lower frequency content (Eyre et al., 2019).

Experiments of fault reactivation in underground laboratories show that fault slip induced by fluid injection at the decametric scale is quantitatively consistent with fault slip and frictional properties measured in the laboratory (Cappa et al., 2019). Hydromechanical models building on experimental evidence (Cappa et al., 2019) suggest that initially, at low fluid pressure, the fault has a slightly rate-weakening or neutral behavior but may change to rate strengthening at and near the injection where fluid pressure and critical nucleation length increase. Fault opening and accelerating creep occur in the pressurized area, whereas at its limit and beyond, the fault remains rate weakening or neutral with a critical amount of accumulated shear stress caused by propagating creep, which helps to trigger seismic slip (Fig. 11).

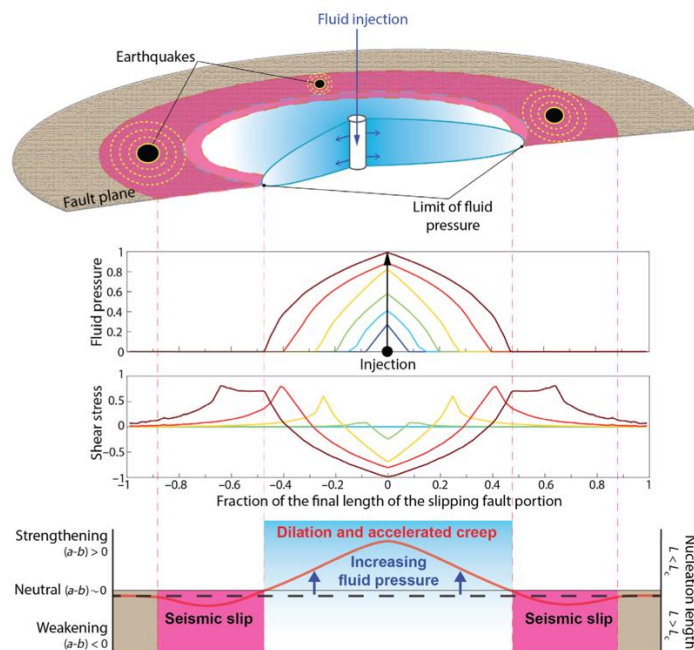


Figure 11. Conceptual illustration of evolution of fault frictional stability during fluid injection derived from experimental evidence and numerical modeling (Cappa et al., 2019).

f) $M_w = 4.1$ during CO₂ sequestration at Castor site revisited (Cesca et al., Nature Communication 2021). The 2013 seismic sequence at the Castor (Spain) with three earthquakes of magnitude 4.1, occurred during the initial filling of a planned Underground Gas Storage facility, is one of the most important cases of induced seismicity in Europe and a rare example of seismicity induced by gas injection into a depleted oil field. Advanced seismological techniques have been used to characterize fault geometry and the temporal evolution of the seismicity (Cesca et al., 2021). Cross-correlation-based relocation, resolve how seismicity is distributed along an elongated volume, extending sub-parallel to the coast with N42°E direction (Fig. 12). Absolute earthquake depths are in the range of 3-4 km and the thickness of the layer affected by seismicity is confined to 2 km only.

The spatiotemporal evolution of seismicity can be divided in three phases. The first begins on September 2, together with the start of the injection, and continues until the injection stops. The second phase begins on September 17 and continues until the end of September and is associated with the evolution of pore pressure and seismicity. These two phases are characterized by different *b*-values, which drops from ~ 1.0 (larger predominance of small earthquakes) to 0.8 (higher rate of larger magnitude events). The third phase, from the end of September to early October, includes all the largest events of the sequence. During the SW migration in phases 1 and 2, which accompanies the spatial extension of the injected gas volume within the NE–SW oriented reservoir, the seismicity rate is discontinuous and small-size earthquakes alternate with short periods of quiescence, leaving large unbroken patches. These are filled by larger earthquakes occurring during phase 3, when seismicity migrates backwards (Fig. 12).

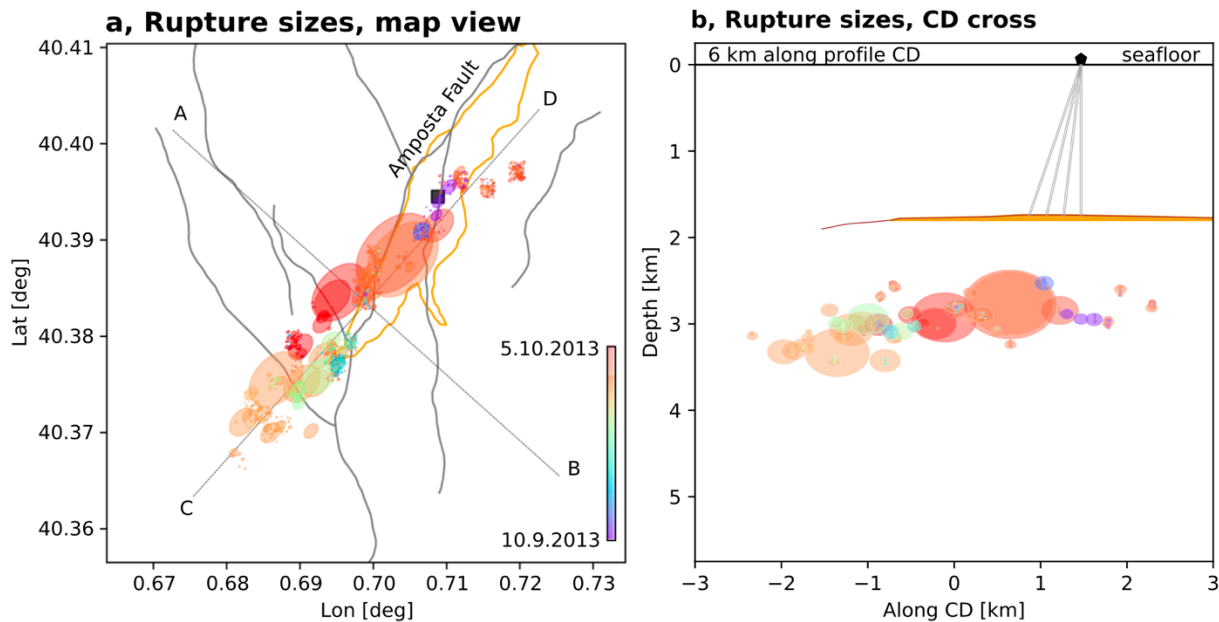


Figure 12. Temporal evolution of the earthquake rupture size: rupture sizes are plotted according to a crack model for a fixed stress drop of 3 MPa (Cesca et al., 2021). The orange line in panel a, marks the approximate outline of the reservoir at the depth of 1800 m and thus the rough extension of the gas-filled volume. A brown line and an orange filled region in panel b sketch the projection of the reservoir roof and gas-filled volume.

- g) CO₂ storage sites with limited induced seismicity
- g1) the UTSIRA formation at the Sleipner gas field

The world's first industrial-scale CO₂ storage operation has been in operation at the Sleipner gas field in the North Sea since 1996. CO₂ is being injected at a depth of about 1000 m into the Utsira Sand, a major, regional saline aquifer (Chadwick et al., 2004). Here a significant amount of CO₂ is coproduced with natural gas. After separating the CO₂ from the produced gas, approximately 1 million tons of CO₂ per year has been injected over the past 15 years without triggering seismicity (Zoback and Gorelick 2012). Assuming isolation from the near surface, injection into highly porous and permeable reservoir that are laterally extensive would produce small increases in pore pressure in response to CO₂ injection (Zoback and Gorelick 2012). In such reservoirs, the stresses relax over time, and such formations are not prone to faulting (Hagin and Zoback, 2004). In this regard, the Utsira formation is ideal for CO₂ sequestration. It is isolated from vertical migration by

impermeable shale formations (Fig. 13), and it is highly porous, permeable, laterally extensive (Fig. 13) and weakly cemented (Zoback and Gorelick 2012).

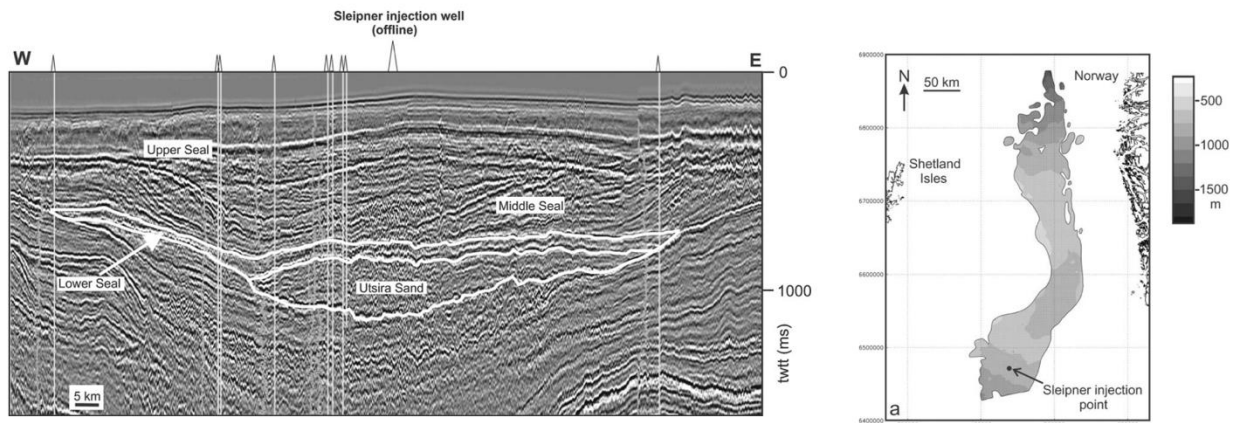


Figure 13. Seismic reflection profile showing the geometry of the Sleipner gas field in the North Sea, with sealing horizons represented by shales, i.e. clay rich lithologies, and the reservoir within the Utsira sand (left figure). Geometry of the Utsira reservoir extending for more than 400 km from north to south and between 50 and 100 km from east to west (from Chadwick et al., 2004).

g2) Long-term sequestration of CO₂ can potentially work in depleted oil and gas reservoirs (Delaware USA).

In the Delaware Basin (western Texas and southeastern New Mexico, USA), pore pressure and stress changes resulting from several decades of oil and gas production significantly affect the likelihood of injection-related induced seismicity (Dvory and Zoback, 2021). Waste-water injection and hydraulic fracturing have been inducing numerous earthquakes in the southernmost part of the basin where there has been no prior oil and gas production (Fig. 14). On the contrary in the formations that experienced oil and gas production no or a few seismicity is occurring. Seismological and INSAR data have been integrated to propose that seismic and aseismic fault motion in the southeastern Delaware Basin, i.e. in the part of the basin where there has been no prior production from, is likely driven by wastewater injection in near critically-stressed normal faults (Pepin et al., 2022). In the part that experienced oil and gas production, the reduction of the least principal stress S_{hmin} with depletion in normal faulting areas tends to suppress the tendency of normal faulting and hence makes induced seismicity less likely (Dvory and Zoback, 2021). Analyses such as this will be

essential in evaluating the potential for long-term sequestration of CO₂ in depleted oil and gas reservoirs and thoroughly evaluating potential seismic hazards.

Production wells in the Delaware Mountain Group, DMG, purple dots

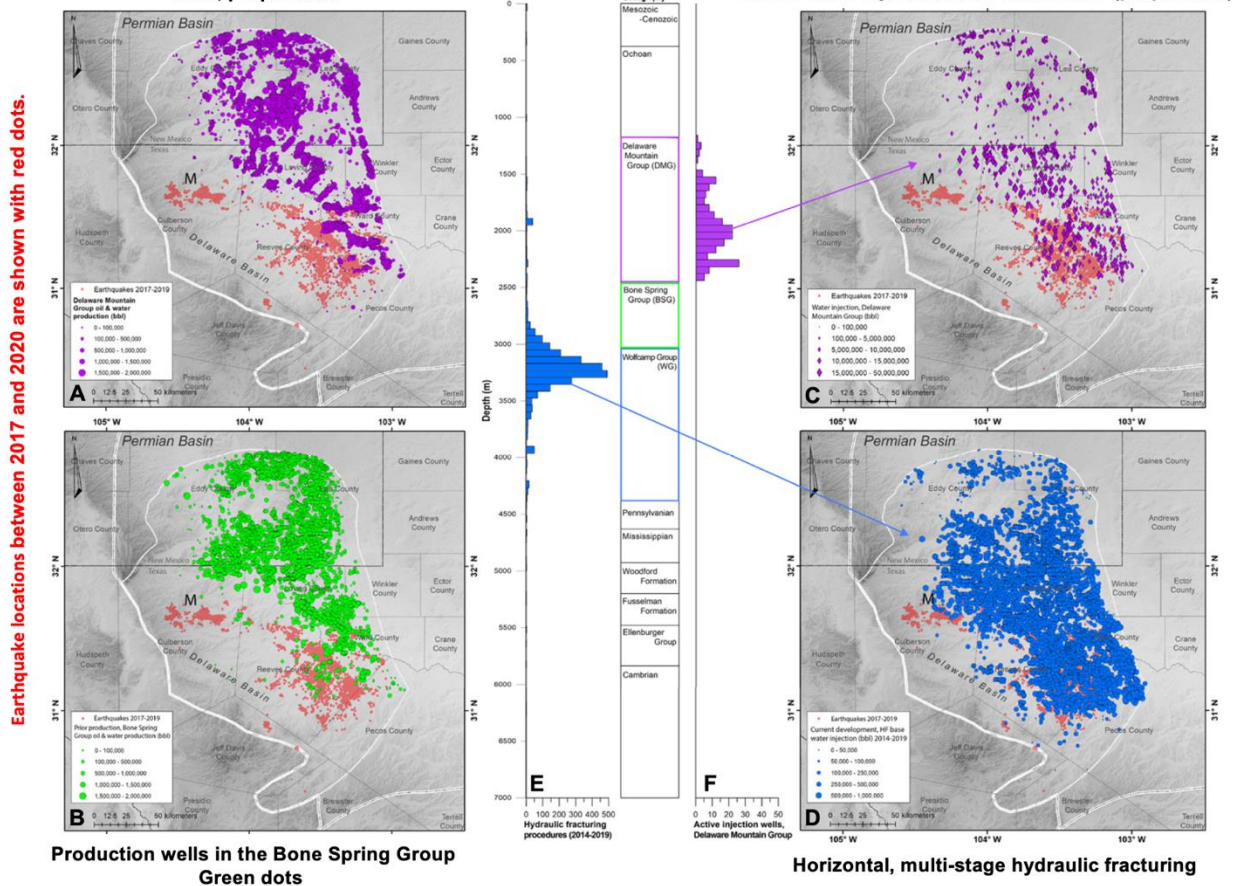


Figure 14. Location of seismicity and wells drilled in the Delaware Basin, western Texas and southeastern New Mexico (USA). From Dvory and Zoback, 2021.

5 Summary of lessons from the case studies of induced seismicity reported in this document

- If the injected fluids from the sedimentary rocks reach the basement a very small increase of pore fluid pressure can trigger earthquakes since many faults within the basement are critically stressed.
- Near–real-time monitoring, and analysis of seismic data are crucial to find a possible road to controlling fluid-pressure induced seismicity. However, differences in tectonics, reservoir and stress conditions can produce significantly different earthquake magnitudes and a runaway rupture.
- High b -values in the Gutenberg-Richter law are likely associated with normal fluid-pressure induced fracture propagation, while smaller b -values can be diagnostic of earthquakes occurring as reactivation of a tectonic fault.
- Fluid-pressure induced aseismic slip along rate-strengthening faults can increase stress on the surrounding regions and promotes earthquakes.
- Injection into highly porous and permeable reservoirs that are laterally extensive would produce small increases in pore pressure in response to injection. In addition, safe accumulation can potentially work in depleted oil and gas reservoirs, e.g. the Delaware case study in USA (Dvory and Zoback, 2021).

References

- Bentz, S., Kwiatek, G., Martínez- Garzón, P., Bohnhoff, M., & Dresen, G.. (2020). Seismic moment evolution during hydraulic stimulations. *Geophysical Research Letters*, 47, e2019GL086185.
- Buijze, AJL. Numerical and experimental simulation of fault reactivation and earthquake rupture applied to induced seismicity in the Groningen gas field. PhD thesis at Utrecht University (2022).
- Cappa, F., Scuderi, M.M., Collettini, C., Guglielmi, Y., Avouac, J.P., 2019. Stabilization of fault slip by fluid injection in the laboratory and in situ. *Sci. Adv.* [https:// doi.org/10.1126/sciadv.aau4065](https://doi.org/10.1126/sciadv.aau4065).
- Cesca et al., Seismicity at the Castor gas reservoir driven by pore pressure diffusion and asperities loading. *Nature Communications*, (2021)12:4783, <https://doi.org/10.1038/s41467-021-24949-1> (2021).
- Chadwick et al., Geological reservoir characterization of a CO₂ storage site: The Utsira Sand, Sleipner, northern North Sea. *Energy* 29 (2004) 1371–1381.
- Collettini C., Cardellini C, Chiodini G, De Paola N, Holdsworth R.E. and Smith S.A.F (2008). Fault weakening due to CO₂ involvement in the extension of the Northern Apennines: short- and long-term processes. *Journal of the Geological Society, Spec. Pub.* 299, 175-194, ISSN: 0016-7649.
- Cousineau, K., Lay, T. & Brodsky, E. E. Two Foreshock Sequences Post Gulia and Wiemer (2019). *Seismol. Res. Lett.* 91, 2843–2850 (2020).
- Dost et al., Development of seismicity and probabilistic hazard assessment for the Groningen gas field. *Netherlands Journal of Geosciences — Geologie en Mijnbouw* |96 – 5 | s235–s245 | (2017).
- Dvory N. Z. and Zoback M. D. Prior oil and gas production can limit the occurrence of injection-induced seismicity: A case study in the Delaware Basin of western Texas and southeastern New Mexico, USA. *Geology* v. 49, p. 1198–1203, (2021).

Ellsworth, W. L. Injection-induced earthquakes. *Science*, (2013).

Ellsworth, W. L., et al., 2015. Increasing seismicity in the U.S. midcontinent: Implications for earthquake hazard: *The Leading Edge*, 34, no. 6, 618–626, <https://doi.org/10.1190/tle34060618.1>.

Ellsworth, W. L., Giardini, D., Townend, J., Ge, S., & Shimamoto, T. Triggering of the Pohang, Korea, earthquake (Mw 5.5) by Enhanced Geothermal System stimulation. *Seismological Research Letters* (2019).

Eyre, T.S., Eaton, D.W., Garagash, D.I., Zecevic, M., Venieri, M., Weir, R., Lawton, D.C., 2019. The role of aseismic slip in hydraulic fracturing–induced seismicity. *Sci. Adv.* 5 (8) eaav7172.

Galis, M., J.P.Ampuero, P.M.Mai, F.Cappa, Induced seismicity provides insight into why earthquake ruptures stop. *Sci. Adv.* 3, eaap7528 (2017).

Goebel, T. H., Kwiatek, G., Becker, T. W., Brodsky, E. E. & Dresen, G. What allows seismic events to grow big?: Insights from b-value and fault roughness analysis in laboratory stick-slip experiments. *Geology* 45, 815–818 (2017).

Gulia, L. & Wiemer, S. Real-time discrimination of earthquake foreshocks and aftershocks. *Nature* 574, 193-199 (2019).

Hgin, P. and Zoback, M.D. Viscous deformation of unconsolidated sands – Part I: Time-dependent deformation, frequency dispersion, and attenuation. *Geophysics*, 69, 731-741.

Keranen, K. M., M. Weingarten, G. A. Abers, B. A. Bekins, and S. Ge, 2014, Induced earthquakes: Sharp increase in central Oklahoma seismicity since 2008 induced by massive wastewater injection: *Science*, 345, no. 6195, 448–451, <https://doi.org/10.1126/science.1255802>.

Kettlety et al., Investigating the role of elastostatic stress transfer during hydraulic fracturing-induced fault activation. *Geophys. J. Int.* (2019) 217, 1200–1216.

Kwiatek, G., et al. Controlling fluid-induced seismicity during a 6.1-km-deep geothermal stimulation in Finland. *Sci. Adv.* 5, eaav7224 (2019).

McGarr, A., Bekins, B., Burkardt, N., Dewey, J., Earle, P., Ellsworth, W., Ge, S., Hickman, S., Holland, A., Majer, E. Coping with earthquakes induced by fluid injection. *Science*, 347, 6224 (2015).

Pepin, K. S., Ellsworth, W. L., Sheng, Y., & Zebker, H. A. (2022). Shallow aseismic slip in the Delaware Basin determined by Sentinel-1 InSAR. *Journal of Geophysical Research: Solid Earth*, 127, e2021JB023157. <https://doi.org/10.1029/2021JB023157>.

Rohmer, J., Plumakers, A. & Renard, F. Mechano-chemical interactions in sedimentary rocks in the context of CO₂ storage: Weak acid, weak effects? *Earth Science Reviews*, 157, 86–110, 2016.

Samuelson, J., Spiers, C.J., Fault friction and slip stability not affected by Co₂ storage: Evidence from short-term laboratory experiments on North Sea reservoir sandstones and caprocks. *Int. J. Greenhouse Gas Control* (2012), <http://dx.doi.org/10.1016/j.ijggc.2012.09.018>.

Scholz, C. H. *The mechanics of earthquakes and faulting.* (Cambridge University Press, 2019).

Schoenball et al., 2018. How faults wake up: The Guthrie-Langston, Oklahoma earthquakes. *THE LEADING EDGE*. <https://doi.org/10.1190/tle37020810.1>.

Schorlemmer, D., Wiemer, S. & Wyss, M. Variations in earthquake-size distribution across different stress regimes. *Nature* 437, 539–542 (2005).

Scuderi, M.M., Collettini, C. 2018. Fluid Injection and the Mechanics of Frictional Stability of Shale-Bearing Faults. *Journal of Geophysical Research, Solid Earth*, 23. <https://doi.org/10.1029/2018JB016084>.

Shelly, D.R., Ellsworth, W. L., & Hill D.P.. Fluid-faulting evolution in high definition: Connecting fault structure and frequency-magnitude variations during the 2014 Long Valley Caldera, California, earthquake swarm. *J. Geophys. Res. Solid Earth* 121, 1776–1795 (2016).

Spetzler J and Dost B. Hypocentre estimation of induced earthquakes in Groningen. *Geophys. J. Int.* (2017) 209, 453–465.

Van Eijs, R., 2015, Neotectonic Stresses in the Permian Slochteren Formation of the Groningen Field: NAM, Koninklijk Nederlands Meteorologisch Instituut Scientific Report EP201510210531.

Verberne et al., 2020. Drill core from seismically active sandstone gas reservoir yields clues to internal deformation mechanisms. *Geology*, 2020, <https://doi.org/10.1130/G48243.1>.

Zoback, M.R. and Gorelick, S. Earthquake triggering and large scale geological storage of carbon dioxide. *PNAS*, June 26, vol. 109, 2012.

Walsh, F. R. III, and M. D. Zoback, 2015, Oklahoma's recent earthquakes and saltwater disposal: *Science Advances*, 1, no. 5, <https://doi.org/10.1126/sciadv.1500195>.

Wyllacy et al., Application of full-waveform event location and moment-tensor inversion for Groningen induced seismicity. *The Leading Edge* (2018) 37 (2): 92–99.
<https://doi.org/10.1190/tle37020092.1>